Viscosity of bimodal and polydisperse colloidal suspensions

Robert A. Lionberger*
Department of Chemical Engineering, University of Michigan, Ann Arbor, Michigan 48109-2136
(Received 22 May 2001; published 21 June 2002)

We present a theoretical framework for the viscosity of bimodal and polydisperse colloidal suspensions. For colloidal dispersions both interparticle forces between pairs of particles and many-particle effects such as depletion forces can have a significant effect on rheology. As hydrodynamic interactions are also important for colloidal systems, a theoretical description that includes hydrodynamic and thermodynamic interactions is required. An integral equation theory for multicomponent systems accounts for the contribution of thermodynamic interactions to the viscosity of dispersions. Introduction of small particles into a system of larger particles causes depletion forces between the large particles that increase the viscosity, while replacing large particles with an equal volume fraction of small particles increases the free volume in the system and decreases the viscosity. The integral equations model both of these effects in concentrated suspensions and provide a microscopic interpretation of free volume changes as changes in radial distribution functions. For a bimodal mixture they predict a dependence of the viscosity on size ratio, composition, and total volume fraction. Polydispersity is modeled by a small number of components whose sizes and weights are chosen to match the moments of the size distribution. This theory predicts a reduction in viscosity due to polydispersity and explains conflicting experimental measurement of the viscosity of hard-sphere colloids. Existing theoretical approaches that neglect the multiparticle correlations, included through the integral equations, yield qualitatively incorrect results for the change in the viscosity relative to monodisperse systems.

DOI: 10.1103/PhysRevE.65.061408 PACS number(s): 82.70.Dd, 83.80.Hj, 61.20.Gy

I. INTRODUCTION

One way to control the viscosity of dispersed systems is to change the size distribution. Often the goal is to lower the dispersion viscosity while maintaining a high volume fraction, as in ceramic processing. There have been many experimental studies of this effect [1–7], some modeling [8,9], and a few simulations [10–12] which were limited to two-dimensional systems. The primary focus has been on noncolloidal particles, but colloidal forces and Brownian motion become important features as particle sizes decrease [13].

This paper applies thermodynamic and hydrodynamic approximations developed previously [14,15] to provide a microscopic description of the effect of mixing different sized Brownian particles on the dispersion viscosity. For hard-sphere interaction potentials the variables affecting the viscosity are the total volume fraction ϕ, size ratio λ, and the fraction by volume of large particles X_L. The questions of interest are as follows. When does mixing different sized particles lead to a minimum of viscosity? What relative fraction of large and small particles leads to the lowest viscosity and how does this depend on total volume fraction and size ratio? How deep is the minimum in viscosity and how does this depth depend on the parameters?

The most important question is the mechanism for the decrease in viscosity. For noncolloidal particles the mechanism is purely hydrodynamic in origin, while for smaller particles Brownian and interparticle forces also contribute. The goal of the theory is to distinguish these effects and compare Brownian particles and noncolloidal particles.

To focus on the three parameters identified above, this paper presents results for the hard-sphere potential only, although the theory is applicable to any interparticle potential. For hard spheres, systems of all large or all small particles at the same volume fraction have the same viscosity, while most other realistic colloidal interactions cause the viscosity of the pure small particles to be higher. This type of theory is also applicable to mixtures of colloidal particles and nonabsorbing polymer.

II. THEORETICAL MODELING

A numerically solvable theoretical description will relate the suspension properties to the microstructure at the level of pair correlations. The primary function characterizing the microstructure is the pair correlation function: $g_{ab}(r)$ in the isotropic equilibrium state and $p_{ab}(\boldsymbol{r})$ in a nonisotropic sheared state. There is one of these functions for each pair of components in the system.

Our approach considers a many-particle system suspended in a solvent, with viscosity μ, interacting through a pairwise additive potential $\Phi_{ab}(r)$. A rigorous approach would require large scale numerical simulation of the motion of a large number of particles coupled to the flow of fluid between them. Through appropriate self-consistent averaging we replace the *N*-body system by a representative pair of particles in a solvent, with viscosity $\eta_{eff} \gg \mu$, interacting through a potential of mean force, Φ_{mf}. The solutions of equations describing this two-particle system yield predictions for the pair correlation function and the viscosity of the suspension.

The self-consistent statistical averaging requires that the properties of the effective medium be coupled to the solution for the correlation functions of the pair of particles. In a multicomponent mixture this couples the pair correlation

*Electronic address: lionberg@umich.edu

functions of the different sized particles together.

A. Equilibrium theory

Recent work applying equilibrium statistical mechanics to mixtures of different sized colloidal particles has been motivated by interest in locating a possible equilibrium phase separation of large and small particles. The first theories of mixtures of hard spheres [16,17] predicted that hard spheres of different sizes would always mix. More current experiments on colloid stability and phase separation [18–20], direct measurements of colloidal forces [21,22], calculations of expected depletion forces from both simulations [23,24] and integral equations [25–27], and other thermodynamic modeling [28,29] have suggested that the depletion forces can cause an entropically driven phase separation.

Exclusion of the small particles from the region between the large particles induces an effective force between the large particles. This force is the potential of mean force, Φ_{aa}^{mf}, between the large particles and can be calculated from the distribution of the large particles,

$$g_{aa}(r)=\exp(-\Phi_{aa}^{mf}/kT). \tag{1}$$

Asakura and Oosawa [30] first calculated this force for the case where the small particles do not interact with each other and the concentration of large particles is dilute and they found

$$\Phi_{aa}^{mf}=-kT\phi_s\left(1+\frac{a_a}{a_b}\right)\left(1+\frac{3}{4}\rho+\frac{1}{16}\rho^3\right),\quad \rho=\frac{r}{a_a+a_b}. \tag{2}$$

This result indicates the attractive nature of the induced interaction and suggests the possibility of an equilibrium phase separation.

For realistic colloidal systems where the small particles interact with each other and the large particles are at a nondilute concentration, an accurate model for $g_{aa}(r)$ is required to invert Eq. (1). Integral equations can provide this information for a wide range of interparticle interactions.

As for monodisperse systems, the starting point for integral equation models is the Ornstein-Zernike equation, which defines the direct correlation function, c_{ab}, through

$$h_{ab}(\boldsymbol{r}_{12})=c_{ab}(\boldsymbol{r}_{12})+\sum_c n_c\int c_{ac}(\boldsymbol{r}_{13})h_{bc}(\boldsymbol{r}_{32})d\boldsymbol{x}_3, \tag{3}$$

where $h_{ab}(\boldsymbol{r}_{12})=p_{ab}(\boldsymbol{r}_{12})-1$. For each pair of components there is one equation and thus an equivalent number of additional equations (a closure) is required to allow solution for all h_{ab}.

The most common closure approximations are the Percus-Yevick (PY) equation

$$h_{ab}(\boldsymbol{r}_{12})=\exp(-\Phi_{ab}/k_bT)[h_{ab}(\boldsymbol{r}_{12})-c_{ab}(\boldsymbol{r}_{12})]-1 \tag{4}$$

and the hypernetted chain (HNC) equation

$$h_{ab}(\boldsymbol{r}_{12})=\exp[-\Phi_{ab}/k_bT+h_{ab}(\boldsymbol{r}_{12})-c_{ab}(\boldsymbol{r}_{12})]-1. \tag{5}$$

The Rogers and Young (RY) equation [31],

$$h_{ab}(\boldsymbol{r}_{12})=\exp(-\Phi_{ab}/k_bT)\times\left[1+\frac{\exp(f_{ab}(r)[h_{ab}(\boldsymbol{r}_{12})-c_{ab}(\boldsymbol{r}_{12})])-1}{f_{ab}(r)}\right]-1, \tag{6}$$

mixes the HNC and PY solution with an adjustable parameter, α in $f_{ab}(r)=1-\exp(-\alpha/\sigma_{ab}r)$, chosen to force agreement between equations of state derived from the pressure and compressibility.

All the integral equations provide quantitatively correct results at small size ratios and low total volume fractions. They indicate the shortcoming of the Asakura-Oosawa model and predict a depletion force that is long ranged and oscillates between attraction and repulsion forces as the separation changes. At larger size ratios and higher total volume fractions, limitations of the closures become apparent and they provide differing predictions of possible phase separations.

For the PY closure there is an analytical solution for mixtures of arbitrary numbers of particles [17]. However, for certain parameters this solution has regions where $g_{ab}(r)$ is negative and thus unphysical. In these regions the equation of state can still be evaluated, however, we cannot use the PY $g(r)$ to calculate the potential of mean force. As a consequence of the negative $g(r)$, which effectively reduces the density of the system, overlapping hard spheres will be less likely and the PY equation predicts that hard spheres of different sizes will always mix. The HNC closure never gives negative $g(r)$, however its numerical solution becomes difficult at higher densities. The RY solution gives much better agreement with equations of state from computer simulation at higher densities, but also combines the limitations of the other closures. Its thermodynamically consistent solutions are not guaranteed to have positive $g(r)$. For example, the RY solutions presented in the work of Hansen and Biben [25,26] yield reasonable values for the equation of state, but also include negative values of $g(r)$ in the region of the first minimum. In contrast to the PY result, their RY solution appears to show a limit of the stability of the homogeneous phase, this indicates a phase transition for extreme sized ratios.

For this paper we use the RY closure to determine the equilibrium structures. Our calculations are primarily for moderate sized ratios because at higher densities we encounter negative $g(r)$ and thus, at these state points we are unable to calculate a potential of mean force for use in computing a viscosity.

B. Hydrodynamic functions

As the particles are dispersed in a viscous fluid, interactions of particles with fluid must be included in the modeling. The actual flow fields in the fluid depend on the location of all the particles, forces, and applied flows present. To

compute this result for all configurations is not feasible, thus we must consider the effect of the fluid averaged over an ensemble of configurations.

A theory for the microscopic dynamics requires a relation between the forces acting on particles and their velocity. For an isolated particle, this relation is simple,

$$\boldsymbol{U}=\frac{D_a^o}{kT}\boldsymbol{F},\quad D_a^o=\frac{kT}{6\pi\mu a}, \tag{7}$$

with the dependence on the particle radius and solvent viscosity closely related to the diffusion coefficient of an isolated particle of radius a,D_a^o. In concentrated suspensions, the presence of the other particles reduces the velocity by a factor proportional to the short time self-diffusion coefficient of a particle of radius a, $D_a^s(\phi)$, where $D_a^s(\phi)<D_a^o$,

$$\boldsymbol{U}=\frac{D_a^s(\phi)}{kT}\boldsymbol{F}. \tag{8}$$

The relative motion of a pair of particles is more complex, even in the dilute limit it depends on the separation as

$$\boldsymbol{U}_r=\boldsymbol{D}_{ab}^r\cdot\boldsymbol{F}_r, \tag{9}$$

with

$$\boldsymbol{D}_{ab}^r=D_{ab}^o\left[G_{ab}\frac{\boldsymbol{rr}}{r^2}+H_{ab}\left(\boldsymbol{\delta}-\frac{\boldsymbol{rr}}{r^2}\right)\right]. \tag{10}$$

The proportionality constant D_{ab}^o is the sum of the diffusion coefficients of particles of sizes a and b,

$$D_{ab}^o=(D_a^o+D_b^o)=\frac{d_a+d_b}{3\pi\mu d_a d_b}. \tag{11}$$

For two isolated particles G_{ab} and H_{ab} are well tabulated [32,33] and asymptote to unity at large separations, corresponding to the independent motion of isolated particles as in Eq. (7), and vanishing at zero separation because of lubrication forces. This relative diffusivity can be measured using optical tweezers and video microscopy [34,35] and is required to interpret scattering measurements of the wave-vector dependent diffusion coefficients in particle mixtures [36].

We also require the relation between the velocity of a particle and the rate of strain tensor, $\boldsymbol{E}$, externally applied to the system. By definition the average velocity of a particle must be that of the average flow at the position $\boldsymbol{x}$,

$$\langle\boldsymbol{U}\rangle=\boldsymbol{E}\cdot\boldsymbol{x}. \tag{12}$$

This must be true for all concentrations. However, the relative velocity of a pair of particles in a flow field does depend on their separation and the suspension concentration via

$$\boldsymbol{U}_r=\boldsymbol{E}\cdot\boldsymbol{r}+\langle\boldsymbol{C}_{ab}^{flow}\rangle_2:\boldsymbol{E}, \tag{13}$$

with

$$\langle\boldsymbol{C}_{ab}^{flow}\rangle_2:\boldsymbol{E}=-r\left[\frac{\boldsymbol{rr}\cdot E\cdot\boldsymbol{r}}{r^3}A_{ab}+\left(\boldsymbol{\delta}-\frac{\boldsymbol{rr}}{r^2}\right)\cdot\frac{\boldsymbol{E}\cdot\boldsymbol{r}}{r}B_{ab}\right], \tag{14}$$

and

$$\begin{aligned}\boldsymbol{\nabla}\cdot(\langle\boldsymbol{C}_{ab}^{flow}\rangle_2:\boldsymbol{E})&=W_{ab}\frac{\boldsymbol{r}\cdot E\cdot\boldsymbol{r}}{r^2}\\&=\left(-3A_{ab}+3B_{ab}-r\frac{dA_{ab}}{dr}\right)\frac{\boldsymbol{r}\cdot E\cdot\boldsymbol{r}}{r^2}.\end{aligned} \tag{15}$$

Again, for two isolated particles A_{ab} and B_{ab} are well tabulated and asymptote at large separations to the isolated particle limit, while at small separation lubrication forces prevent relative motion of the pair.

For monodisperse suspensions at high concentrations, the most effective existing models for the hydrodynamic interaction functions originated when Medina-Noyola [37] and Brady [38] first recognized that the known values of the short-time diffusion coefficient could be used to rescale the results of dynamical theories that did not include hydrodynamic interactions. The success of this approximation is best understood in terms of the known asymptotic forms of the hydrodynamic interaction functions. At large separations the pair of particles moves independently and the function must asymptote to the result of the single-particle averaging: for example, $G(r)\to D_s^o(\phi)$ at large r. At small separation the solvent viscosity determines the relative motion through a lubrication analysis. An interpretation of these limits is that the pair of particles feels an effective viscosity equal to the solvent viscosity near contact and equal to the tracer particle value at large separations. In between these limits the effective viscosity varies with separation, as indicated by the oscillation in $G(r)$. At high density the dominant effect is the reduction in magnitude which is captured by the far-field value. Brady's and Medina-Noyola's rescaling applies this far-field result at all separations. Figure 1 shows a comparison of the far-field result to a Stokesian dynamics calculation to test the quality of the approximation. Upon changing the concentration from $\phi=0$ to $\phi=0.3$, the diffusion coefficient decreases and the absolute difference between the far-field approximation and the exact result decrease, explaining much of the success of the approximation in concentrated suspensions [39]. Thus, we employ the far-field rescaling for all further calculations

$$G_{ab}=\frac{D_{ab}^s(\phi)}{D_{ab}^o}\begin{cases}0 & r=\frac{1}{2}(d_a+d_b)\\ 1 & r>\frac{1}{2}(d_a+d_b)\end{cases}\qquad H_{ab}=\frac{D_{ab}^s(\phi)}{D_{ab}^o},$$

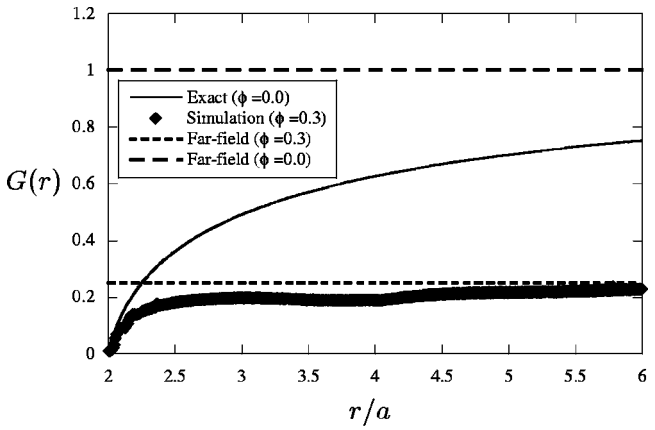

FIG. 1. Exact results for $G(r)$ are obtained from Stokesian dynamics simulation and plotted at $\phi=0.0$ and $\phi=0.3$. The comparison of the far-field prediction with these results shows a great improvement in the far-field approximation as the volume fraction increases.

$$A_{ab}=\begin{cases}1 & r=\frac{1}{2}(d_a+d_b)\\ 0 & r>\frac{1}{2}(d_a+d_b)\end{cases}\qquad B_{ab}=0. \tag{16}$$

To apply the far-field rescaling to mixtures of different sized particles we extend the dilute suspension mixing rule in Eq. (10) to

$$D^s_{ab}(\phi)=[D^s_a(\phi)+D^s_b(\phi)]. \tag{17}$$

C. Nonequilibrium theory for weak flows

To predict the viscosity, the integral equation approach must be extended to account for the distortion of the equilibrium structure due to the applied flow. The first attempt at using integral equations to account for the dynamics of bimodal dispersions was by Ohtsuki [8]. Our integral equation approach begins with the integration [14] of an N-particle conservation equation over the positions of all but two particles, to produce an equation for the pair distribution function that accounts for interparticle, hydrodynamic, and Brownian forces,

$$\frac{\partial p(\boldsymbol{r}_{12})}{\partial t}+\boldsymbol{\nabla}\cdot\left[p(\boldsymbol{r}_{12})(\boldsymbol{\Gamma}\cdot\boldsymbol{r}+\langle\boldsymbol{C}^{flow}\rangle_2:\boldsymbol{E})+\frac{1}{k_bT}\langle\boldsymbol{D}^r\rangle\cdot[p(\boldsymbol{r}_{12})\times\langle\boldsymbol{F}^r\rangle_2-\boldsymbol{\nabla}p(\boldsymbol{r}_{12})]\right]=0. \tag{18}$$

$\boldsymbol{\Gamma}$ is the velocity gradient tensor of an applied flow and the rate of strain tensor is its symmetric part as $\boldsymbol{E}=\frac{1}{2}(\boldsymbol{\Gamma}+\boldsymbol{\Gamma}^T)$. This equation includes conditional averages of interparticle forces, $\langle\boldsymbol{F}^r\rangle_2$ and hydrodynamic interactions, $\langle\boldsymbol{D}^r\rangle_2$ and $\langle\boldsymbol{C}^{flow}\rangle_2$, defined by

$$P_2(\boldsymbol{x}_1,\boldsymbol{x}_2)\langle A\rangle_2=N(N-1)\int AP_N d\boldsymbol{x}_3\cdots d\boldsymbol{x}_N, \tag{19}$$

where $P_2(\boldsymbol{x}_1,\boldsymbol{x}_2)=n(\boldsymbol{x}_1)n(\boldsymbol{x}_2)p(\boldsymbol{r}_{12})$. Additional thermodynamic and hydrodynamic approximations for these conditional averages are required to solve the model [15].

The modification of the equation presented above to treat mixtures of different sized particles must recognize the different pair potentials, Φ_{ab}, between each pairwise combination of particles in the system. For hard spheres this is not complicated, but for other potentials the strength of the interaction may depend on both the relative and absolute particle sizes. The pair potential gives rise to different distribution functions for each possible pair of particles, $p_{ab}(\boldsymbol{r})$. To generalize the monodisperse case, we derive a two-particle equation for each $p_{ab}(\boldsymbol{r})$,

$$\frac{\partial p_{ab}(\boldsymbol{r}_{12})}{\partial t}+\boldsymbol{\nabla}\cdot\left[p_{ab}(\boldsymbol{r}_{12})(\boldsymbol{\Gamma}\cdot\boldsymbol{r}+\langle\boldsymbol{C}^{flow}_{ab}\rangle_2:\boldsymbol{E})+\frac{1}{k_bT}\langle\boldsymbol{D}^r_{ab}\rangle\cdot[p_{ab}(\boldsymbol{r}_{12})\langle\boldsymbol{F}^r_{ab}\rangle_2-\boldsymbol{\nabla}p(\boldsymbol{r}_{12})]\right]=0. \tag{20}$$

These equations also require thermodynamic and hydrodynamic closures, but in a multicomponent mixture the closures can couple the pair correlation functions of different sized particles. For example, the conditional averages of the interparticle forces now have the form

$$p_{ab}\langle\boldsymbol{F}^r_{ab}\rangle_2=-p_{ab}\boldsymbol{\nabla}_1\Phi_{ab}(\boldsymbol{r}_{12})-\frac{1}{2}\sum_c n_c\int p_{abc}[\boldsymbol{\nabla}_1\Phi_{ac}(\boldsymbol{r}_{13})-\boldsymbol{\nabla}_2\Phi_{bc}(\boldsymbol{r}_{23})]d\boldsymbol{x}_3, \tag{21}$$

which includes a sum over the all other types of particles in the system.

We consider the three thermodynamic closures with the pair approximation

$$\langle\boldsymbol{F}^r_{ab}\rangle_2=-\boldsymbol{\nabla}\Phi_{ab}\,(\text{Pair}) \tag{22}$$

completely decoupling the set of conservation equations. The mean force approximation [40]

$$\langle\boldsymbol{F}^r_{ab}\rangle_2=-\boldsymbol{\nabla}\Phi^{mf}_{ab}=k_bT\boldsymbol{\nabla}\ \ln\ g_{ab}(r,\phi)\quad(\text{Mean Force}) \tag{23}$$

includes an equilibrium coupling between different sizes. The integral closure,

$$k_bTp(\boldsymbol{r}_{12})\langle\boldsymbol{F}^r_{ab}\rangle_2=\boldsymbol{C}_{ab}(\boldsymbol{r}_{12})+\frac{1}{2}\sum_c n_c\int[\boldsymbol{C}_{ac}(\boldsymbol{r}_{13})h_{bc}(\boldsymbol{r}_{32})+\boldsymbol{C}_{bc}(\boldsymbol{r}_{23})h_{ac}(\boldsymbol{r}_{31})]d\boldsymbol{x}_3, \tag{24}$$

adds a self-consistent nonequilibrium coupling, but requires another equation for $\boldsymbol{C}_{ab}$,

$$\boldsymbol{C}_{ab}(\boldsymbol{r}_{12})=-p_{ab}(\boldsymbol{r}_{12})\boldsymbol{\nabla}_1\Phi(\boldsymbol{r}_{12})+h_{ab}(\boldsymbol{r}_{12})\boldsymbol{Q}_{ab}(\boldsymbol{r}_{12})\quad(\text{Integral}), \tag{25}$$

where

$$\boldsymbol{Q}_{ab}(\boldsymbol{r}_{12}) = \frac{1}{2}\sum_c n_c \int [\boldsymbol{C}_{ac}(\boldsymbol{r}_{13})h_{bc}(\boldsymbol{r}_{32}) + \boldsymbol{C}_{bc}(\boldsymbol{r}_{23})h_{ac}(\boldsymbol{r}_{31})]d\boldsymbol{x}_3. \tag{26}$$

In a previous paper [14] we showed that the integral approximation described perturbations of the equilibrium pair distribution function, which are equivalent to the imposition of an arbitrary pairwise additive external potential $\Phi^{fict}(\boldsymbol{r})$. This potential does not appear explicitly in the final equations and at equilibrium, when $\Phi^{fict}(\boldsymbol{r})=0$ the integral approximation reduces to the standard HNC equilibrium closure. This formalism allows us to calculate the response of the equilibrium structure to a weak flow and thus determine the low shear Newtonian viscosity of the suspension.

The total stress in a suspension can be separated into a hydrodynamic contribution $\boldsymbol{\Sigma}^H$ and a thermodynamic contribution $\boldsymbol{\Sigma}^T$. To leading order in shear rate the hydrodynamic contribution represents an ensemble average over the equilibrium distribution function. Exact results from Batchelor, and Green with renormalization of conditionally convergent integrals, exist only to $O(\phi^2)$ [41]. However, measurements of the high frequency viscosity provide values of this contribution as

$$\boldsymbol{\Sigma}^H = 2\eta'_\infty \boldsymbol{E} + O(\boldsymbol{E}:\boldsymbol{E}). \tag{27}$$

The thermodynamic stress

$$\boldsymbol{\Sigma}^T = \frac{1}{2}\sum_{a,b} n_a n_b \int (1-A_{ab})\boldsymbol{r}\boldsymbol{\nabla}\Phi_{ab}p_{ab}d\boldsymbol{r} - \frac{1}{2}k_bT\sum_{a,b} n_a n_b \int W_{ab}\frac{\boldsymbol{rr}}{r^2}p_{ab}d\boldsymbol{r}, \tag{28}$$

is caused by the perturbation of the suspension microstructure from equilibrium by the applied flow.

For a weak shear flow, the perturbation of the pair distibution from equilibrium has the form

$$p_{ab}(\boldsymbol{r}_{12}) = g_{ab}(r)\left(1+\frac{\boldsymbol{r}\cdot\boldsymbol{E}\cdot\boldsymbol{r}}{r^2}f_{ab}(r)\right). \tag{29}$$

A solution for f_{ab} is required to determine the coefficient between stress and strain rate.

For the integral closure expansion of the function Q,

$$\boldsymbol{Q}_{ab}(\boldsymbol{r}_{12}) = \boldsymbol{\nabla}\Phi^{mf}_{ab} - \boldsymbol{\nabla}\Phi^{12}_{ab} + \frac{\boldsymbol{r}\cdot\boldsymbol{E}}{r}\cdot\left[\frac{\boldsymbol{rr}}{r^2}Q^{\parallel}_{ab}(r) + \left(\boldsymbol{\delta}-\frac{\boldsymbol{rr}}{r^2}\right)Q^{\perp}_{ab}(r)\right]$$

is required, while for the other closures $\boldsymbol{Q}_{ab}=0$. Substituting these expansions into Eq. (20), leaves the final conservation equation

$$\frac{1}{\bar{r}^2}\frac{d}{d\bar{r}}\bar{r}^2 G_{ab}\left(\frac{d\bar{f}_{ab}}{d\bar{r}}-\bar{Q}^{\parallel}_{ab}\right) - \frac{6H_{ab}}{\bar{r}^2}\left(\bar{f}_{ab}-\tfrac{1}{2}\bar{Q}^{\perp}_{ab}\right) - G_{ab}\frac{d\bar{\Phi}^{mf}_{ab}}{d\bar{r}}\left(\frac{d\bar{f}_{ab}}{d\bar{r}}-\bar{Q}^{\parallel}_{ab}\right) = \frac{D^o_0}{D^o_{ab}}\left(-\bar{r}(1-A_{ab})\frac{d\bar{\Phi}^{mf}_{ab}}{d\bar{r}}+W_{ab}\right), \tag{30}$$

and boundary condition at the ab overlap distance, d_{ab},

$$G_{ab}\left(\frac{d\bar{f}_{ab}}{d\bar{r}}-\bar{Q}^{\parallel}_{ab}\right) = \frac{D^o_0}{D^o_{ab}}\bar{r}(1-A_{ab}), \tag{31}$$

with dimensionless variables

$$\bar{r}=\frac{r}{L_0},\quad \bar{f}_{ab}=\frac{D^o_0 f_{ab}}{L_0^2},$$

$$\bar{\Phi}^{mf}_{ab}=\frac{\Phi^{mf}_{ab}}{k_bT},\quad \bar{Q}^{\parallel}_{ab}=\frac{D^o_0 Q^{\parallel}_{ab}}{L_0 k_b T},\quad \bar{Q}^{\perp}_{ab}=\frac{D^o_0 Q^{\perp}_{ab}}{L_0 k_b T},$$

$$Pe=\frac{L_0^2\gamma}{D^o_0},\quad D^o_0=\frac{kT}{3\pi\mu L_0},\quad \gamma=(\boldsymbol{E}:\boldsymbol{E})^{1/2}, \tag{32}$$

with L_0 the diameter of the largest particle.

When we employ the simple hydrodynamic approximation from Eq. (16) the equations simplify to

$$\frac{1}{\bar{r}^2}\frac{d}{d\bar{r}}\bar{r}^2\left(\frac{d\bar{f}_{ab}}{d\bar{r}}-\bar{Q}^{\parallel}_{ab}\right) - \frac{6}{\bar{r}^2}\left(\bar{f}_{ab}-\tfrac{1}{2}\bar{Q}^{\perp}_{ab}\right) - \frac{d\bar{\Phi}^{mf}_{ab}}{d\bar{r}}\left(\frac{d\bar{f}_{ab}}{d\bar{r}}-\bar{Q}^{\parallel}_{ab}\right) = -\bar{r}\frac{D^o_0}{D^s_{ab}(\phi)}\frac{d\bar{\Phi}^{mf}_{ab}}{d\bar{r}}, \tag{33}$$

with no-flux boundary condition at the ab overlap distance

$$\frac{d\bar{f}_{ab}}{d\bar{r}}-\bar{Q}^{\parallel}_{ab} = \frac{D^o_0}{D^s_{ab}(\phi)}\bar{r}. \tag{34}$$

In the integral approximation these equations are coupled and thus require a complicated numerical scheme to find a self-consistent solution. The mean-force approximation results in independent conservation equations, which require a numerical solution and input of the potential of mean force from the equilibrium integral equations. For hard spheres, the pair approximation leads to an analytical solution.

For all the closures the viscosity of a hard-sphere suspension is related to the nonequilibrium structure through

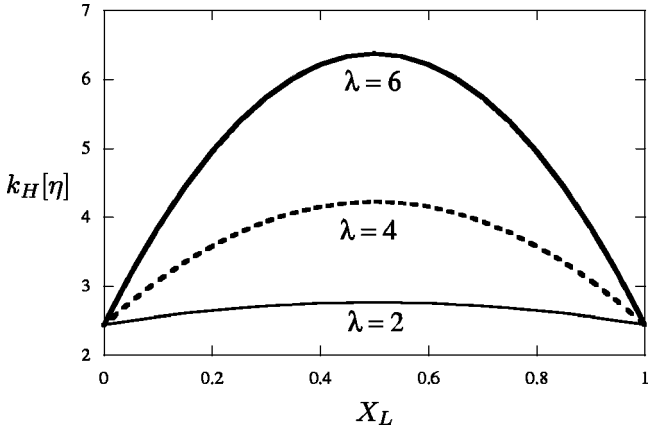

FIG. 2. Examination of the thermodynamic contribution to the $O(\phi^2)$ term in the expansion of the viscosity shows that in the dilute limit the far-field hydrodynamic interactions lead to a viscosity maximum.

$$\frac{\eta}{\mu}=\frac{\eta'_\infty}{\mu}+\frac{72}{5}\sum_{ab}\frac{D_0^o}{D_{ab}^s(\phi)}\phi_a\phi_b\left(\frac{L_0}{d_a}\right)^3\left(\frac{L_0}{d_b}\right)^3 \times f_{ab}(d_{ab})g_{ab}(d_{ab}), \tag{35}$$

with the factor $D_0^o/D_{ab}^s(\phi)$ accounting for the reduced mobility due to hydrodynamic interactions. This hydrodynamic approximation replaces the characteristic relative mobility at low densities D_{ab}^o with the volume fraction dependent scale $D_{ab}^s(\phi)$.

III. RESULTS

A. Viscosity of bimodal suspensions

We first calculate the viscosity of bimodal suspensions with the three thermodynamic closures to test their applicability to multicomponent mixtures. All thermodynamic closures reduce to the pair closure in the dilute limit where exact calculations are possible, first performed by Wagner and Wouterson [42]. Figures 2 and 3 show that with the far-field hydrodynamic interactions there is a viscosity maximum that increases with increasing size ratio. Exact two-particle hydrodynamic interactions convert the maximum to a minimum that deepens with the size ratio. We expect that the quality of the far-field hydrodynamic approximation will increase with increasing density. The figures plot the viscosity reduced via

$$k_H[\eta]=\frac{\frac{\eta_0}{\mu}-1-[\eta]\phi}{\phi^2},\quad [\eta]=\frac{5}{2}, \tag{36}$$

to remove the terms that are independent of the particle size.

In Figs. 4–6 we use the far-field hydrodynamic approximation combined with various thermodynamic approximations, as in Fig. 2 this hydrodynamic approximation leads to a viscosity maximum at low density where all of the thermodynamic approximations are identical. Figure 4 shows that the pair closure predicts an increase in the viscosity for all volume fractions and simply amplifies the trends in the dilute limit. By including only the pair potential, it neglects the effect of other particles on the force and misses its coupling to the density. The other thermodynamic closures (Figs. 5 and 6) include this coupling which converts the viscosity maximum for low volume fraction into the expected mini-

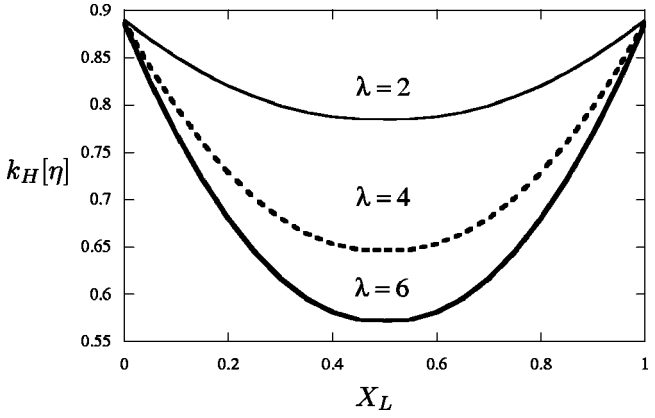

FIG. 3. Examination of the thermodynamic contribution to the $O(\phi^2)$ term in the expansion of the viscosity shows that exact hydrodynamic interactions lead to a viscosity minimum.

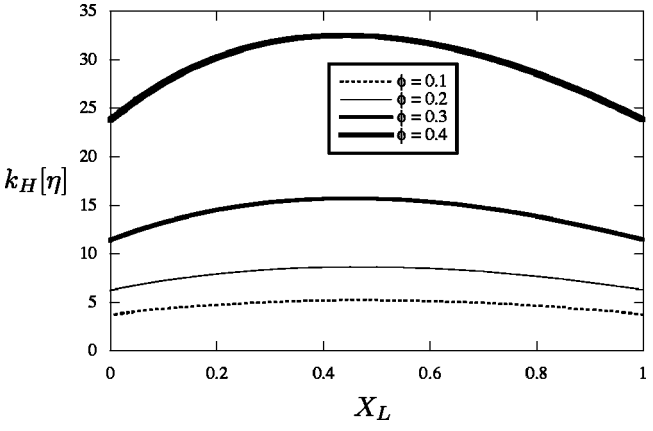

FIG. 4. The viscosity for size ratio 3:1 as a function of volume fraction using the pair thermodynamic closure.

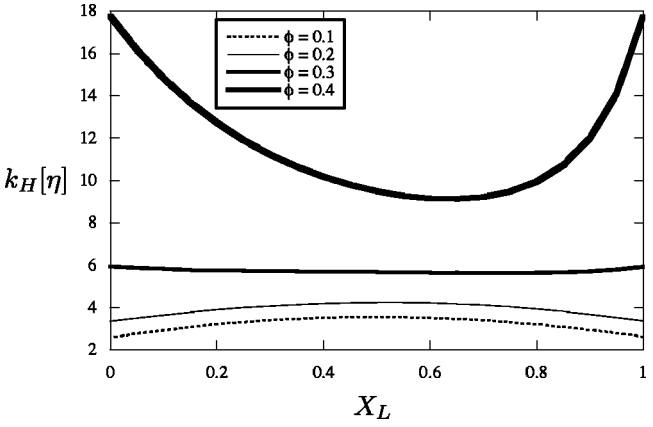

FIG. 5. The viscosity for size ratio 3:1 as a function of volume fraction using the mean force thermodynamic closure.

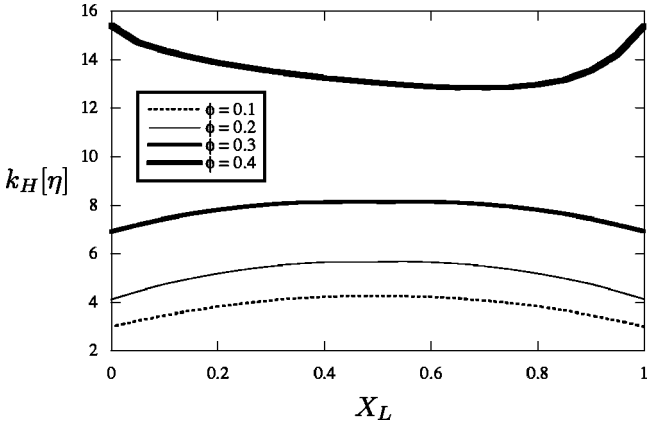

FIG. 6. The viscosity for size ratio 3:1 as a function of volume fraction using the integral thermodynamic closure.

mum at a higher volume fraction. The coupling to density has two manifestations. First, the viscosity decreases because replacing large particles with an equal volume of small particles increases the free volume, which allows the smaller particles to access interstitial space inaccessible to large particles. In the radial distibution functions this is seen as the large-small and small-small correlation functions in the mixture having smaller peaks than the correlation functions in a monodisperse system at the same volume fraction. Second, the viscosity increases because the small particles increase the viscosity of the medium and cause depletion forces that induce an effective attraction between large particles. The location and depth of the viscosity minimum is determined by a balance between these two effects.

A quantitative validation of this approach is provided by comparison with two sets of experimental results for bimodal hard-sphere colloidal suspensions. Shikata [43] fixed the total volume fraction and varied the composition for two different sized ratios, while Rodriguez [44] varied the total volume fraction and composition with the size ratio fixed. Shikata's silica particles deviate from hard-sphere behavior as they show a difference in the viscosities of the pure components, but the data and theory in Fig. 7 show similar mag-

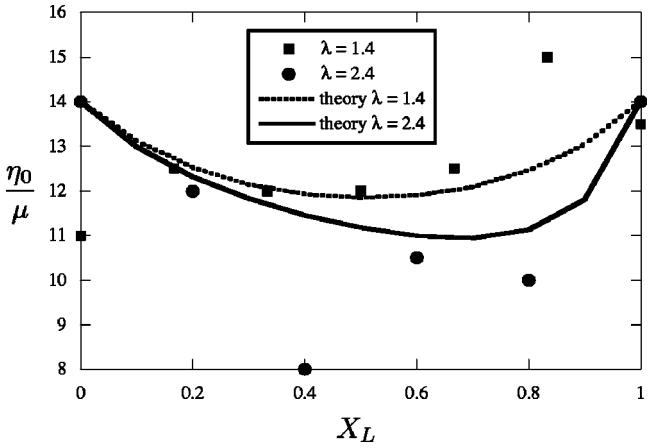

FIG. 7. Comparison of integral closure at $\phi = 0.46$ with the data of Shikata [43] for size ratios of 1.4 and 2.4.

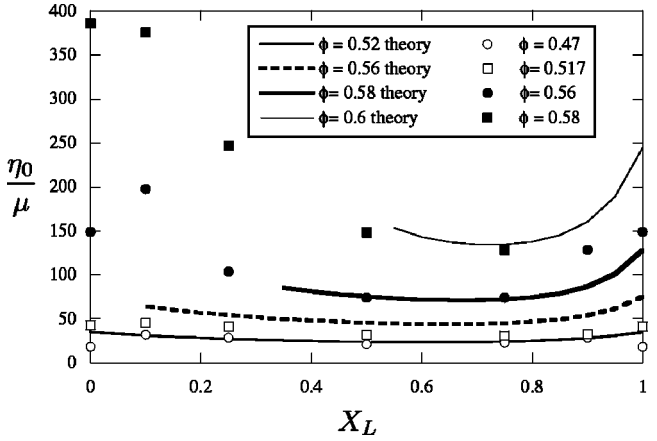

FIG. 8. Comparison of integral closure at a size ratio of 1.67 with the volume fraction dependence of the data of Rodriguez, *et al.* [44].

nitudes for the viscosity decrease and the shift in the location of the minimum with a change in the size ratio. The other data in Fig. 8 show that the theory also predicts the change in magnitude and minimum with increasing volume fraction. At the highest volume fraction the predicted curves terminate when we can no longer solve the equilibrium integral equations. In this region the depletion forces are causing too strong an attraction between the large particles for the integral equations to be successful.

Neither of the data sets corresponds exactly to the predicted behavior for hard-spheres. Shikata's data has several points where the viscosity of the mixed system is higher than the pure components and Rodriguez's data have viscosities of the pure components that are not equal at equal volume fractions as required for hard spheres. There are several possible explanations for these observations. The inequality of pure components could be caused by a nonhard-sphere interactions, with the consequence that smaller particles would have a higher viscosity. Another possible cause of the difference in viscosity is due to the shear rate dependence of the viscosity. Beyond a critical Pe the viscosity will begin to decrease with shear rate. This critical Pe decreases with volume fraction, thereby making experimental measurement of the low shear viscosity difficult at high volume fraction. The critical Pe also decreases with particle size. So at nonzero shear rates the viscosity for large particles will be less than for small ones. For example, the data of Bender and Wagner [45] for higher shear rates illustrate this effect as their viscosity versus composition plots have a strong dependence on shear rate. Both of these effects would tend to increase the viscosity of the small particles relative to the large particles. Other mechanisms that could cause systematic deviations from predicted hard-sphere behavior include wall-particle interactions, especially depletion forces that would preferential by change the composition near the walls.

B. Comparison of colloidal and noncolloidal models

There are several existing empirical approaches to modeling the viscosity of particle mixtures with most of them

having been first developed for noncolloidal particles. Comparison to the rigorous theory indicates that they have a limited range of validity and illustrates important differences between colloidal and noncolloidal particles.

Rodriguez [44] and Chang and Powell [10] correlate their viscosities, from experiments and simulations, respectively, via the same form often used for the viscosity of monodisperse suspensions

$$\eta \propto (\phi - \phi_{max})^{-2}. \tag{37}$$

For bimodal mixtures, the maximum packing fraction, ϕ_{max}, is a function of the size ratio but not of total volume fraction. A consequence of this model is that it always predicts a viscosity minimum and this minimum is always at the same composition regardless of total volume fraction. This is inconsistent with theory and experiment which show that the location of a maximum or minimum depends on total volume fraction. Thus, this model should only be considered valid at volume fractions near maximum packing. Another limitation is that the determination of the maximum packing fraction is difficult even for monodisperse hard-spheres and even more ambiguous for particles that are soft. Usually the value of maximum packing is chosen to fit the data and is not determined independently. Our approach has the same behavior near maximum packing and identifies the ϕ_{max} with the divergence of the osmotic pressure of a mixture of colloidal particles.

A different approach, first employed by Farris [46,47] treats the small particles as a continuum. This is obviously only valid for large differences in particle size. The expression for the viscosity of a monodisperse suspension is

$$\frac{\eta_{suspension}}{\eta_{solvent}} = \eta_{mono}(\phi). \tag{38}$$

$\eta_{mono}(\phi)$ is the function that describes the volume fraction dependence of the relative viscosity of a monodisperse hard-sphere suspension. This function is used twice. First, consider the small particles as the solvent for the large particles,

$$\frac{\eta_{suspension}}{\eta_{small}} = \eta_{mono}(\phi_L). \tag{39}$$

Second, we use Eq. (38) for η_{small},

$$\frac{\eta_{small}}{\mu} = \eta_{mono}\left(\frac{\phi_S}{1-\phi_L}\right), \tag{40}$$

with the viscosity of the small particle phase calculated with a volume fraction based on the space not occupied by the large particles. Combining Eqs. (39) and (40) leaves

$$\frac{\eta_{suspension}}{\mu} = \eta_{mono}\left(\frac{\phi_S}{1-\phi_L}\right)\eta_{mono}(\phi_L). \tag{41}$$

The first limitation of this model is that it does not predict any dependence on particle size. D'haene and Mewis [2] recognized that finite sized particles cannot access the entire free volume of $1-\phi_L$ in the same way a continuum fluid can and so they added an additional adjustable parameter to aid in fitting their data for a size ratio of 6.4. As this model was developed for noncolloidal suspensions, it does not consider depletion forces. As the size of the small particles decreases the force between large particles becomes larger and larger. The consequence of this is that for noncolloidal systems increasing the size ratio leads to a greater decrease in viscosity, while in colloidal systems the maximum decrease in viscosity is limited by the increasing depletion forces. This is a consequence of a mathematical paradox of the hard-sphere model. As the size ratio of a bimodal hard-sphere system goes to infinity, the limit is not a monodisperse hard-sphere suspension. The hard-sphere solvent will always induce a force between hard particles. Experimental colloidal systems that mimic hard-sphere systems do so because the properties of the solvent and particles are carefully tuned to give a delicate cancellation of van der Waals and excluded volume interactions.

A way to modify the approach of Farris to give the correct behavior for colloidal systems with a large size ratio is to calculate $\eta_{mono}(\phi_L)$ in Eq. (41) using the potential of mean force induced by the solvent particles. This potential of mean force is computed from the integral equations with a fixed volume fraction of small spheres and the large spheres at infinite dilution [23,48].

In the regions rich in large particles, $X_L \cong O(1)$, or rich in small particles, $X_S \cong O(1)$, a lower bound to the viscosity is the ''invisible'' particle limit

$$\eta(X_L, \phi_T) \geqslant \eta_{mono}(\phi_T - \phi_S) = \eta(\phi_L),$$

$$\eta(X_S, \phi_T) \geqslant \eta_{mono}(\phi_T - \phi_L) = \eta(\phi_S), \tag{42}$$

where the minority component excluded volume disappears. Interactions between the dilute particles increase the viscosity from this limit according to their Huggins coefficient as

$$\eta(X_S \approx 1, \phi_T) \approx \eta_{mono}(\phi_S)(1 + [\eta]\phi_L + k_H^L[\eta]\phi_L^2), \tag{43}$$

where ϕ_L is small. At the other end, where ϕ_S is small, the equivalent equation is

$$\eta(X_L \approx 1, \phi_T) \approx \eta_{mono}(\phi_L)(1 + [\eta]\phi_s + k_H^S[\eta]\phi_S^2). \tag{44}$$

We obtain k_H from a solution to Eq. (20) in the limit of the density going to zero and with the pair potential Φ_{12} replaced by the potential of mean force Φ_{mf}. As shown in Fig. 9 the potential of mean force between large particles changes as the size ratio varies and has oscillations on the length scale of the small particle size. There is an increase in the strength of attraction for larger size ratios. In Fig. 10, for the

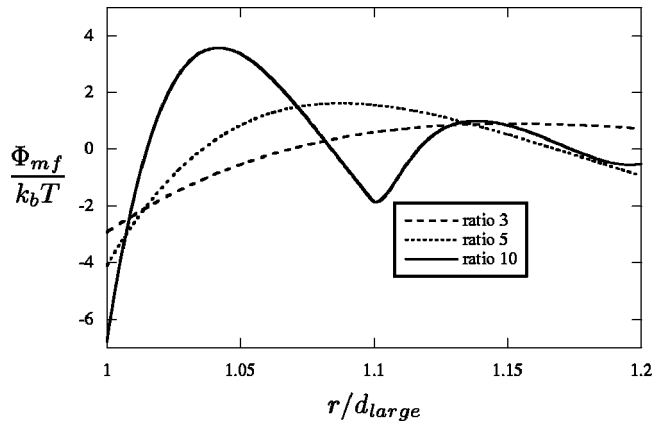

FIG. 9. The potential of mean force between two large particles in a suspension of small particles at $\phi=0.4$ for size ratios of 3, 5, and 10.

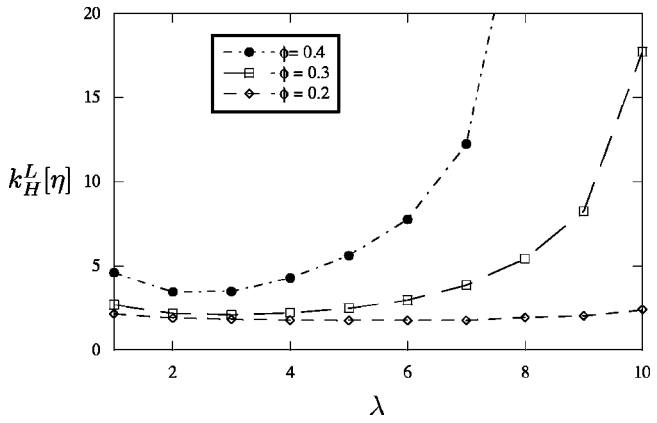

FIG. 11. At several different values of the total volume fraction, the Huggins coefficient for infinity dilute large particles shows a minimum as a function of the size ratio.

inverse situation of small particles in a suspension of large particles, the small particles feel a weaker potential with long-range oscillations. The viscosity reduction when small particles are added to pure large particles is larger than when large particles are added to pure small particles because there are stronger depletion forces induced in the second case, indicated by $k_H^L > k_H^S$.

Examination of k_H^L indicates the importance of depletion forces in colloidal systems. The calculations in Fig. 11 are at fixed total volume fraction and infinite dilution of the large particles. They show the Huggins coefficient has a minimum with respect to size ratio. For large size ratios the Huggins coefficient strongly increases, in accord with the expectation that an increase in the strength of attraction will increase the viscosity [49]. In noncolloidal systems at extreme size ratios where Eq. (43) would be valid, there would be no Huggins coefficient correction from depletion forces and the viscosity is free to decrease until the lower bound. In colloidal systems, an attempt to reduce the viscosity by decreasing the size of the small particles will eventually begin to increase the viscosity at large enough size ratios. Whether a minimum is observed will depend on the balance between stronger depletion force and the viscosity decrease due to an apparent reduction in the volume fraction of the majority component.

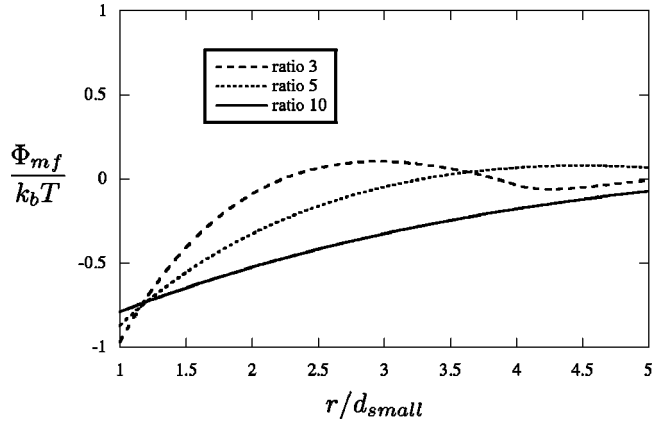

FIG. 10. The potential of mean force between two small particles in a suspension of large particles at $\phi=0.4$ for size ratios of 3, 5, and 10.

C. Viscosity of polydisperse suspensions

To apply our multicomponent theory to a polydisperse suspension we choose the size and number density of p components to match the first $2p$ moments of the distribution of sizes in the suspension [50]. We assume a Schultz distribution of sizes

$$F(\sigma)=\left[\frac{t+1}{\langle\sigma\rangle}\right]^{t+1}\frac{\sigma^t}{\Gamma(t+1)}\exp\left(-(t+1)\frac{\sigma}{\langle\sigma\rangle}\right), \quad (45)$$

where σ is the particle diameter and $\langle\sigma\rangle$ its average, Γ is the gamma function, and $t=(1-s^2)/s^2$ with s being the standard deviation of the particle size about the mean. The Schultz distribution is convenient because its moments are governed by a simple recurrence relation.

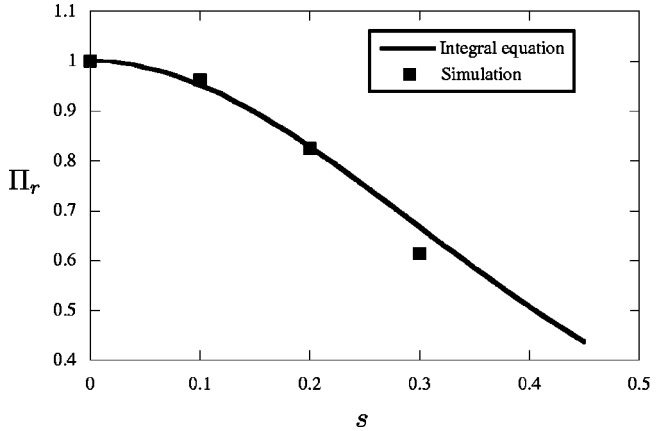

FIG. 12. Comparison of the pressure from the PY integral equation [normalized on the monodisperse pressure, $\Pi_r=\Pi(s)/\Pi(s=0)$] at $\phi=0.5$ with that measured in simulation by Rastogi *et al.* [51].

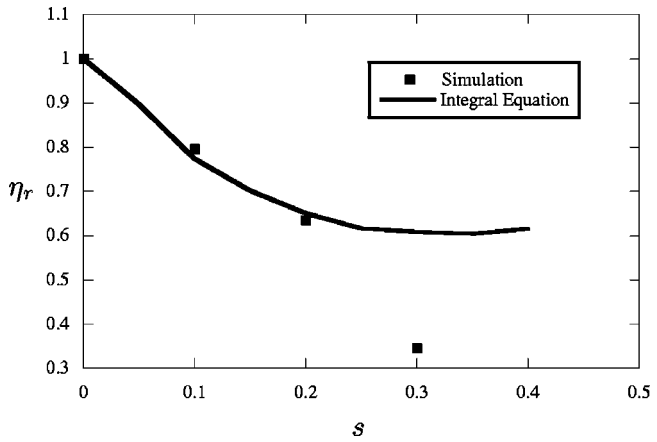

FIG. 13. Comparison of the viscosity from the integral closure [normalized on the monodisperse viscosity, $\eta_r = \eta(s)/\eta(s=0)$] at $\phi = 0.5$ with that measured in simulation by Rastogi *et al.* [51].

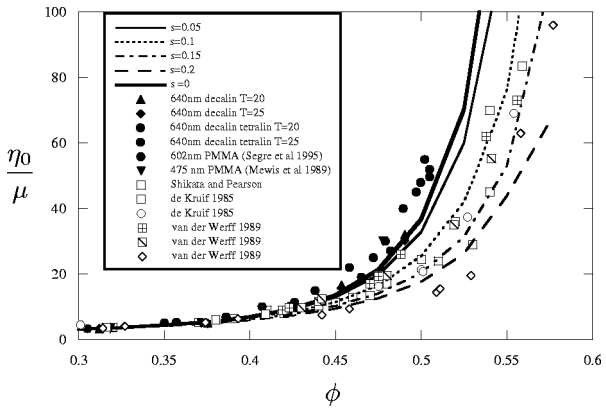

FIG. 14. Comparison of the viscosity from the mean force closure as a function of ϕ for a range of polydispersities compared to the measurements from de Kruiff *et al.* [56], van der Werff *et al.* [57], Mewis *et al.* [58], Shikata and Pearson [59], Segré *et al.* [60], and Phan *et al.* [54].

To validate the polydisperse model, we first compare the theory to Rastogi's [51] simulations of charge-stabilized colloids, which neglected hydrodynamic interactions. The pressure in Fig. 12 shows excellent agreement between the simulation and integral equation theory. The PY results depend only on the first three moments of a continuous size distribution and thus are exactly reproduced by our multicomponent approximation. For the viscosity in Fig. 13, we see very good agreement for low polydispersities with deviation between theory and simulation at larger values of s, indicating that the viscosity has a more complicated dependence on the size distribution than the pressure. Thus the multicomponent approximation is only practical for modest polydispersities. Improvement of the approximation through the addition of more components to match more moments is not feasible as the size ratio between the largest and smallest components becomes too large for the existing numerical method.

Figure 14 shows the prediction for hard-spheres with hydrodynamic interactions compared with several sets of experimental data. The experimental results appear to fall into two classes of materials. The data sets with higher viscosities are for PMMA particles that are monodisperse enough to form colloidal crystals at volume fractions greater than $\phi = 0.5$. The data sets with lower viscosities are a variety of materials but share the common feature that they are not observed to form colloidal crystals and are believed to be of higher polydispersity. Kofke and Bolhuis [52,53] suggest that for hard-spheres there is critical polydispersity of about 10% beyond which the fluid will not crystallize. The polydispersity of the PMMA systems [54] is clearly below this value while the other systems could exceed this threshold. All the experimental systems claim to have a hard-sphere interaction potential. Previously polydispersity has been suggested [55] as a possible explanation for this division of the experimental data. Our calculations demonstrate this effect quantitatively and show that the difference between these two classes of materials can be explained by the effect of polydispersity on viscosity, as shown in the theoretical curves on the plot. The conclusion is that the PMMA data should be considered to most closely represent the viscosity for monodisperse hard-spheres.

IV. CONCLUSIONS

This paper illustrates that both the integral and mean force closures capture the qualitative behavior of mixtures of different sized particles. The simpler pair closure that succeeds for monodisperse mixtures gives quantitatively incorrect results, primarily because of the importance of three particle (depletion) interactions in mixtures. A recent analysis of the Smoluchowski approach to colloid dynamics [61] using the GENERIC formalism [62,63] demonstrated that the integral and mean force closures as used here are thermodynamically consistent while the pair closure is not. The fact that the pair closure predicts a nonphysical increase in viscosity and is thermodynamically inconsistent indicates the utility of the GENERIC formalism.

Some of the features of bimodal mixtures predicted by the thermodynamically consistent models are as follows. (1) A viscosity minimum (as a function of composition) at low volume fractions with full hydrodynamic interactions becomes a viscosity maximum when only far-field hydrodynamic interactions are included; (2) a transition from viscosity maximum to viscosity minimum (again as a function of composition) occurs at a total volume fraction of about $\phi = 0.4$ when far-field hydrodynamic interactions are employed; (3) the dependence of the composition at the minimum viscosity on particle size ratio and total volume fraction; (4) the magnitude of the viscosity minimum as a function of total volume fraction, size ratio, and composition; and (5) the reduction of viscosity caused by polydispersity.

The models for multicomponent mixtures can easily be extended to other interparticle potentials, but at present solutions are limited to size ratios and densities for which existing integral equations yield realistic values of the potentials of mean force. A direct calculation of the depletion forces from simulation could provide the missing information.

[1] A.T.J.M. Woutersen and C.G. de Kruif, J. Rheol. **37**, 681 (1993).
[2] P. D'Haene and J. Mewis, Rheol. Acta **33**, 165 (1994).
[3] W. Richtering and H. Muller, Langmuir **11**, 3699 (1995).
[4] W.J. Hunt and C.F. Zukoski, Langmuir **12**, 6257 (1996).
[5] A.A. Zaman, B.M. Moudgil, A.L. Fricke, and H. Elshall, J. Rheol. **40**, 1191 (1996).
[6] P. Gondret and L. Petit, J. Rheol. **41**, 1261 (1997).
[7] R. Greenwood, P.F. Luckham, and T. Gregory, J. Colloid Interface Sci. **191**, 11 (1997).
[8] T. Ohtsuki, Physica A **122**, 212 (1983).
[9] G. Nagele and J. Bergenholtz, J. Chem. Phys. **108**, 9893 (1998).
[10] C.Y. Chang and R.L. Powell, J. Fluid Mech. **253**, 1 (1993).
[11] C.Y. Chang and R.L. Powell, J. Rheol. **38**, 85 (1994).
[12] C.Y. Chang and R.L. Powell, Phys. Fluids **6**, 1628 (1994).
[13] R.L. Hoffman, J. Rheol. **36**, 947 (1992).
[14] R.A. Lionberger and W.B. Russel, J. Chem. Phys. **106**, 402 (1997).
[15] R.A. Lionberger and W.B. Russel, J. Rheol. **41**, 399 (1997).
[16] J.L. Lebowitz and J.S. Rowlinson, J. Chem. Phys. **41**, 133 (1964).
[17] J.L. Lebowitz, Phys. Rev. **133**, A895 (1964).
[18] J. van Duijneveldt, A. Heinen, and H. Lekkerkerker, Europhys. Lett. **21**, 369 (1993).
[19] P.D. Kaplan, J.L. Rouke, A.G. Yodh, and D.J. Pine, Phys. Rev. Lett. **72**, 582 (1994).
[20] A.D. Dinsmore, A.G. Yodh, and D.J. Pine, Phys. Rev. E **52**, 4045 (1995).
[21] X.L. Chu, D. Nikolov, and D.T. Wasan, Langmuir **12**, 5004 (1996).
[22] W. Xu, D. Nikolov, and D.T. Wasan, AIChE J. **43**, 3215 (1997).
[23] T. Biben, P. Bladon, and D. Frenkel, J. Phys.: Condens. Matter **8**, 10 799 (1996).
[24] R. Dickman, P. Attard, and V. Simonian, J. Chem. Phys. **107**, 205 (1997).
[25] T. Biben and J.-P. Hansen, Europhys. Lett. **12**, 347 (1990).
[26] T. Biben and J.P. Hansen, Phys. Rev. Lett. **66**, 2215 (1991).
[27] C. Caccamo and G. Pellicane, Physica A **235**, 149 (1997).
[28] W. Poon and P.B. Warren, Europhys. Lett. **28**, 513 (1994).
[29] A. Konig and N.W. Ashcroft, Phys. Rev. E **63**, 041203 (2001).
[30] S. Asakura and F. Oosawa, J. Polym. Sci. **33**, 183 (1958).
[31] F.J. Rogers and D.A. Young, Phys. Rev. A **30**, 999 (1984).
[32] D. Jeffrey and Y. Onishi, J. Fluid Mech. **139**, 261 (1984).
[33] D. Jeffrey, Phys. Fluids A **4**, 16 (1992).
[34] J.C. Crocker, J. Chem. Phys. **106**, 2837 (1997).
[35] R.V. Durand and C. Franck, Phys. Rev. E **56**, 1998 (1997).
[36] P.D. Kaplan, A.G. Yodh, and D.J. Pine, Phys. Rev. Lett. **68**, 393 (1992).
[37] M. Medina-Noyola, Phys. Rev. Lett. **60**, 2705 (1988).
[38] J.F. Brady, J. Chem. Phys. **98**, 3335 (1993).
[39] S.R. Rastogi and N.J. Wagner, J. Rheol. **41**, 893 (1997).
[40] W.B. Russel and A.P. Gast, J. Chem. Phys. **84**, 1815 (1986).
[41] G.K. Batchelor and J.T. Green, J. Fluid Mech. **56**, 401 (1972).
[42] N. Wagner and A. Woutersen, J. Fluid Mech. **278**, 267 (1994).
[43] T. Shikata, H. Niwa, and Y. Morishima, J. Rheol. **42**, 765 (1998).
[44] B.E. Rodriguez, E.W. Kaler, and M.S. Wolfe, Langmuir **8**, 2382 (1992).
[45] J. Bender and N.J. Wagner, J. Rheol. **40**, 899 (1996).
[46] R.J. Farris, Trans. Soc. Rheol. **12**, 281 (1968).
[47] M.Z. Sengun and R.F. Probstein, J. Rheol. **41**, 811 (1997).
[48] J.G. Malherbe and S. Amokrane, Mol. Phys. **99**, 355 (2001).
[49] W.B. Russel, D.A. Saville, and W.R. Schowalter, *Colloidal Dispersions* (Cambridge University Press, Cambridge, 1989).
[50] B. D'Aguanno and R. Klein, Phys. Rev. A **46**, 7652 (1992).
[51] S.R. Rastogi, N.J. Wagner, and S.R. Lustig, J. Chem. Phys. **104**, 9249 (1996).
[52] P.G. Bolhuis and D.A. Kofke, Phys. Rev. E **54**, 634 (1996).
[53] P.G. Bolhuis and D.A. Kofke, J. Phys.: Condens. Matter **8**, 9627 (1996).
[54] S. Phan *et al.*, Phys. Rev. E **54**, 6633 (1996).
[55] E.G.D. Cohen, R. Verberg, and I.M. de Schepper, Physica A **251**, 251 (1998).
[56] C.G. de Kruiff, E.M. van Iersel, A. Vrij, and W.B. Russel, J. Chem. Phys. **83**, 4717 (1986).
[57] J.C. van der Werff and C.G. de Kruiff, J. Rheol. **33**, 421 (1989).
[58] J. Mewis, W.J. Frith, T.A. Strivens, and W.B. Russel, AIChE J. **35**, 415 (1989).
[59] D.S. Pearson and T. Shikata, J. Rheol. **38**, 601 (1994).
[60] P.N. Segré, S.P. Meeker, P.N. Pusey, and W.C.K. Poon, Phys. Rev. Lett. **75**, 958 (1995).
[61] N.J. Wagner, J. Non-Newtonian Fluid Mech. **96**, 177 (2001).
[62] M. Grmela and H.C. Ottinger, Phys. Rev. E **56**, 6620 (1997).
[63] H.C. Ottinger and M. Grmela, Phys. Rev. E **56**, 6633 (1997).